Journal of Hazardous Materials 480 (2024) 136140

Contents lists available at ScienceDirect

Journal of Hazardous Materials

journal homepage: www.elsevier.com/locate/jhazmat

Adsorption behavior of ZIF-67 to bisphenol compounds affects combined toxicity on *Photobacterium phosphoreum*

Dan Wang [a,b], Linming Bai [a,b], Wenlong Wang [a], Ruixue Zhang [a], Shanshan Li [a,*], Wei Yan [a]

[a] *Xi'an Key Laboratory of Solid Waste Recycling and Resource Recovery, Department of Environmental Science and Engineering, Xi'an Jiaotong University, Xi'an 710049, China*

[b] *China National Key Laboratory of Aerospace Chemical Power, Hubei Institute of Aerospace Chemotechnology, Xiangyang 441003, China*

HIGHLIGHTS

- Combined effects of ZIF-67 and bisphenol compounds (BPA, BPS and BPAF) to *Photobacterium phosphoreum*.
- MOF showed a high adsorption capacity for BPAF and the weakest adsorption capacity for BPA.
- The difference in adsorption capacity for BPs resulted in different amounts of free BPs, contributing to the combined toxicity.
- Oxidative damage and luminescence damage are the main reasons for combined toxicity.

GRAPHICAL ABSTRACT

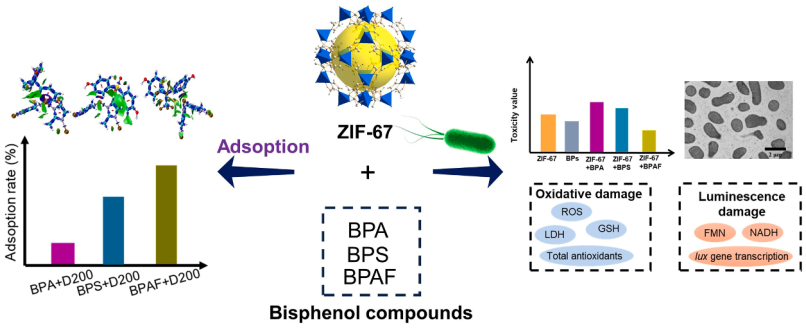

ARTICLE INFO

Keywords:
ZIF-67
Bisphenol compounds
Co-exposure
DFT
Toxicity mechanism

ABSTRACT

ZIF-67, as a typical MOF material, is considered a new type of high-potential adsorbent due to its ample surface area and tunable surface chemistry, which has the potential to interact with other contaminants in unforeseen ways, resulting in combined toxicity. To further elucidate this possibility, we chose typical bisphenol compound (BP) which is widely used in commercial manufacturing, to explore the combined toxicity with MOF. MOF showed a high adsorption capacity for BPAF (> 80 %) and the weakest adsorption capacity for BPA (< 10 %), and DFT confirmed the different interaction strengths of MOF for BPs. The difference in adsorption capacity for BPs resulted in different amounts of free BPs, contributing to combined toxicity. Based on flow cytometry and TEM, the results showed that membrane damage was reduced and the ability of ZIF-67 to enter the cell was decreased in the low-concentration ZIF-67 mixing group, and the ability of ZIF-67 to enter the cell was increased in the high-concentration ZIF-67 mixing group, and the membranes were severely damaged. RT-PCR and biochemical indicators measurements helped to explain the underlying toxicity mechanism. This study is of practical significance for the development of environmental guidelines for mixed contaminant effects and accurate risk assessments.

* Corresponding author.
E-mail address: shanshan0320@xjtu.edu.cn (S. Li).

https://doi.org/10.1016/j.jhazmat.2024.136140
Received 28 July 2024; Received in revised form 15 September 2024; Accepted 9 October 2024
Available online 10 October 2024

1. Introduction

Metal-organic framework (MOF), an ordered three-dimensional structure formed by self-assembly of metal ions and organic ligands, has developed fast and has attracted considerable attention [1-4]. In the last two decades, the total number of publications associated with MOF has increased 66-fold from 147 to nearly 10,000 indexed by Web of Science Core Collection. More than 20,000 MOFs have already been synthesized, with the promise of widespread application [5]. In terms of marketing applications, it is reported that MOF market will reach over $8.9 billion in 2023 and is estimated to reach $27.3 billion in 2032.

Due to the adequate surface area and tunable surface chemistry, MOFs are considered a potential adsorbent widely used for the adsorptive removal of different pollutants [6-8]. This has led to a significant increase in the potential of MOF to come into contact with other pollutants, among which it is worth mentioning the co-exposure scenarios of MOF with bisphenol compounds (BPs). Ahsan et al. synthesized two modified Cu-MOFs (GO-modified Cu-MOFs and CNT-modified Cu-MOFs) to remove the BPA in water. The results showed that the adsorption capacities of the two nanomaterials for BPA were 182.2 and 164.1 mg/g, respectively, which were much higher than the adsorption capacity of Cu-MOF [9]. Yu et al. introduced the porphyrin unit structure into Zr-based MOF using an ultrasonic method and synthesized Zr-based porphyrins MOF-505 and MOF-545, both exhibited excellent high efficiency and high rate of adsorption for BPA [10]. The application of MOF for the detection and degradation of BPA has also been more thoroughly studied. Arul et al. synthesized the Ni-MOF onto amino acid-functionalized graphene nanosheets, showing high sensitivity and stability for BPA [11]. A novel boron and nitrogen-modified peroxymonosulfate activated carbon catalyst (Fe@BPC-XBN) prepared with an iron-based metal-organic skeleton (Fe-MOF) showed promising application prospects by removing 93.3 % of BPA within 90 min [12]. All these developments will inevitably lead to the encounter of MOF and BPs, which may be exposed to organisms and pose a threat to environmental safety.

Bisphenol compounds (BPs) are one of the vital raw materials for synthesizing polymer materials [13]. A large number of studies have revealed that BPs can be detected in food, house dust, environmental samples, human urine, blood and consumer products [14,15]. The most well-known BPs is bisphenol A (BPA). BPA has been identified as a weak estrogenic chemical that binds to estrogen receptors and alters endocrine function in organisms, causing adverse reactions [16]. Many countries have banned the use of BPA as a food utensil additive. Bisphenol S (BPS) and Bisphenol F (BPF) are widely used as alternatives to BPA. Some studies have determined the toxic effects of BPs and evaluated the risks of use [17-20].

More studies have been performed on the toxicity of nanomaterials co-exposure to other pollutants, while there is still a gap in the investigation of the combined toxic effects of MOF and BPs. For example, Liu et al. used the human colorectal mucosal cells to investigate the combined effect of biochars and Cr/As, they found that redox-induced chemical speciation determined the combined toxicity [21]. The large specific surface area and high surface reactivity of nanomaterials make adsorption the most common physicochemical process when nanomaterials are co-exposed with other pollutants. The combined effect of graphene oxide (GO) and Cd^{2+} was studied on *Chlorella vulgaris,* and the results showed that Cd^{2+} was absorbed on the GO surface and the combined toxicity enhanced when two co-exposure [22]. In addition to facilitating the uptake of other pollutants after direct adsorption, it has been found that GO can shift the valence state of arsenic, which in turn increased its toxicity to wheat (*Triticum aestivum* L.) [23]. It can be seen that most nanomaterials do not have a similar toxicity effect after co-exposure with other pollutants due to different physicochemical properties, and there is no universal conclusion that can directly guide toxicity assessments.

In this study, we chose typical cobalt-based MOF (ZIF-67) and three common BPs (BPA, BPS and BPAF) as representative pollutants to explore the combined toxicity effect and toxicity mechanism. The absorption capacities of ZIF-67 to three BPs were experimentally explored and the conclusions were verified based on DFT. The toxicity values of the test group were determined using luminescent bacteria acute toxicity test, a commercially available toxicity test method with sensitivity comparable to the 96-hour acute toxicity test on fish [24,25]. Based on these toxicity data, the content of ZIF-67 and BPs entering the cell were determined, and the toxic contribution of each component in the combined toxicity was clarified. Moreover, flow cytometry and TEM were conducted to evaluate intracellular damage. With the help of quantitative data of typical biochemical indicators and relevant expression of core-related genes, the potential combined toxicity mechanism of ZIF-67 and typical BPs was revealed.

2. Materials and methods

2.1. Materials and bacteria

Sources of chemicals are detailed in the supporting information (Text S1). According to the previous research, ZIF-67 (200 nm, recorded as D200) was prepared [26]. The stock solutions of BPA, BPS, BPF, BPAF, BPB and tetrabromobisphenol A (TBBPA) were prepared in 2 % DMSO solution and stored in −20℃. A certain amount of the above BPs was dissolved in the 3 % NaCl solution and sonicated for 2 min, and the concentrations were set as 100, 50, 25, 10 and 1 mg/L.

The luminescent bacteria *Photobacterium phosphoreum* T3 strain was purchased from China General Microbiological Culture Collection Center (Beijing, China).

2.2. Cell cultivation and toxicity assay

The culture medium and cell cultivation process of T3 strain were according to the previous study [26]. The final cell density of T3 strain in PBS for toxicity assay was 1.5×10^7 CFU/mL. The cells were exposed to the desired test samples and incubated for 15 min. The bioluminescence intensity was determined with a Modulus™ Single Tube Multimode Reader (Turner Biosystems, USA). The Luminescence inhibition rate (LIR) can be calculated and the toxic level estimation was shown as IC_{50}, the calculation methods of LIR and the IC_{50} values obtained by the Weibull function model were according to the previous study [26].

2.3. Adsorption capacity of ZIF-67 for BPs

Different concentrations of ZIF-67 and BPs were prepared according to the experimental design, and the solvent contained DMSO (2 %, v/v). ZIF-67 was mixed with BPs for 15 min, afterwards the mixture solution was filtered by polyethersulfone membrane (0.22 μm). Only the BPs not adsorbed by ZIF-67 were retained in the filtrates. The filtrate was collected and the concentration of BPs in the filtrate was determined by HPLC-MS (iChrom 5100, Elite, China). The chromatographic conditions are detailed in the Text S2. On the basis of adsorption experiment results, the interactions between ZIF-67 and three BPs were explored by Density Functional Theory (DFT). The detailed methodology is described in Text S3.

2.4. Adsorption and separation experiment of intracellular materials

2.4.1. Intracellular adsorption amount of ZIF-67

After the toxicity assay, the T3 strain in the test sample was collected by centrifugation and washed with PBS three times. Then the T3 strain was digested with HNO_3 (65 %, v/v) for 24 h. The concentration of HNO_3 in the sample was diluted to 5 % (v/v), and the intracellular cobalt content of T3 strain was determined by ICP-OES (ICPE-9000, Shimadzu, Japan).

2.4.2. Intracellular distribution of absorbed ZIF-67

The effects of ZIF-67 on cell morphology were observed by transmission electron microscope (TEM, HT7800, Hitachi, Japan). After co-exposure with ZIF and BPs for 30 min, the precipitate was washed with PBS and centrifuged to collect. The procedure for the preparation of test samples was described in previous studies.

2.4.3. The adsorption capacity of intracellular ZIF-67 on BPs

Detailed separation methods are described in Text S4. After 15 min of exposure to T3 strain, the mixture solution containing the T3 strain was filtrated by 0.22 μm filter membrane, collecting the cells on the membrane and the filtrate, respectively. The cells were washed with sterile water and stored at −20℃. The filtrate obtained by filtration was denoted as solution B.

The collected cells were lysed by a freeze-thaw method. After repeated freezing and thawing for 3 times, the bacteria lysed and released the BPs absorbed by bacteria, ZIF-67 absorbed by bacteria and ZIF-67 containing adsorbed BPs absorbed by bacteria. Then, the above mixture solution was filtered with a 0.22 μm filter membrane to remove ZIF-67 (containing ZIF-67 adsorbed with BPs), and the filtrate was collected and denoted as solution A. Solution A only contained intracellular BPs which are not adsorbed by ZIF-67. The BPs content in solution A was determined by HPLC-MS.

BPs not absorbed by bacteria, ZIF-67 not absorbed by bacteria and ZIF-67 containing adsorbed BPs not absorbed by bacteria were all present in solution B. ZIF-67 in solution B was removed by adding HNO_3 and the BPs adsorbed by ZIF-67 were released at the same time. The content of BPs in solution B was determined by HPLC-MS. The amount of the BPs is the total content of the BPs that have not entered the bacteria.

Subtract the content of the BPs measured in solution A from the total BPs content, and then subtract the content of the BPs measured in solution B to obtain the intracellular content of the BPs adsorbed by ZIF-67.

2.5. Determination of the biochemical biomarkers

After the toxicity assay, the collected bacteria were homogenized in NP 40 lysis buffer with sonic treatment for 20 min in an ice bath. The supernatants were stored at −80℃ for the following tests. The FMN and NADH content in the sample were measured using the enzyme-linked immunosorbent assay (ELISA) kits (Ruifan, Shanghai, China) following the manufacturer's instructions. The intracellular ROS production was measured by ELISA kits (Ruifan, Shanghai, China). The Reduced Glutathione (GSH) content and the total antioxidant capacity (T-AOC) in samples were detected using the GSH Colorimetric Assay Kit E-BC-K030-M (Elabscience, China) and T-AOC kit (Beyotime, China), respectively. The lactate dehydrogenase (LDH) activity was measured to reflect the extent of membrane damage using the LDH cytotoxicity assay kit (Beyotime, China), following the manufacturer's instructions.

2.6. Analysis of the percentage of live/dead bacteria

Bacteria were collected by centrifugation after 15 min of exposure to the test material, and the final concentration of bacteria was approximately 1.5×10^7 CFU/mL. The dyeing cell process was followed by our previous work [27]. The two stains, SYTO-9 and propidium iodide (PI), were used to discriminate living and dead bacteria (LIVE/DEAD BacLight Bacterial Viability, Thermo Fisher, USA). In particular, SYTO-9 could stain and label all bacteria. The PI dye, a cytosolic fluorescent dye similar to ethidium bromide, can only penetrate membrane-damaged bacteria, decreasing SYTO-9 stain fluorescence when both dyes are present. The percentage of live/dead bacteria was analyzed using the self-contained program on the flow cytometer (CytoFLEX, Keyi, China) to classify the bacteria into P3 and P4 zones, where P3 zones are membrane-damaged cells and P4 zones are intact live cells. Data analysis was processed by flow cytometry software.

2.7. Real-time quantitative PCR (RT-PCR) analysis

RT-PCR was used to determine the transcription levels of the *lux*A and *lux*B after exposure to the treatment groups. The two genes, *lux*A and *lux*B, are encoded in luciferase, vital to the luminescence process [28]. The primer sequences of the selected gene are shown in Table S1. All RT-PCR measurements were according to the previous research [26].

2.8. Statistical analysis

Data were analyzed with GraphPad Prism (Ver. 7.0; GraphPad Software, California, USA) and presented as the mean ± standard deviation based on triplicate results from three independent experiments. Differences between the control and treated groups were analyzed using the Student's t-test. $p < 0.01$ were denoted significance.

3. Results and discussion

3.1. The single toxicity of ZIF-67 and BPs

The common physicochemical properties and their molecular structure of six BPs (BPA, BPAF, BPF, BPS, BPB and TBBPA) are shown in Table S2 and Fig. S1. By use of the Weibull function fitting, the IC_{50} values for TBBPA, BPAF, BPB, BPS, BPF and BPA were 8.81, 10.02, 11.58, 18.77, 18.38 and 39.04 mg/L (Table S3). The biotoxicity of TBBPA was the highest, followed by BPAF and BPB, the IC_{50} value of BPA was 10 times lower than that of TBBPA. Similar results were found in the study of Tisler et al. They found that the IC_{50} of BPS (2.1 mg/L) was lower than that of BPF (4.2 mg/L) based on luminescent bacteria *V. fischeri*, indicating that BPS was more toxic than BPF [29]. The different single toxicity of BPs may be related to their structural variation and molecular weight [30].

The IC_{50} value for ZIF-67 (200 nm) estimated in our previous investigation, was 4.58 mg/L [26]. Based on the single biotoxicity results and relative molecular weight of six BPs, BPA, BPS and BPAF were selected to investigate the combined effects with ZIF-67. According to the Weibull function fitting, the toxicity order of three BPs was BPAF > BPS > BPA.

3.2. Toxicity assay of ZIF-67 co-exposure with BPs

The test concentrations of BPs are selected based on a concentration corresponding to LIR of about 35–40 %. The 25, 5 and 1 mg/L were determined as the test concentrations for BPA, BPS and BPAF, respectively. In terms of ZIF-67, high (10 mg/L) and low (2 mg/L) concentrations of ZIF-67 (corresponding to the LIR of 75 % and 40 %, respectively) were selected to explore the combined toxicity with the three BPs. Experimental groups are denominated by concentration and compound name. For example, the experimental group of 25 mg/L BPA was recorded as 25 BPA. The nomenclatures of all experimental groups are shown in Table S4.

The results of single and combined toxicity of ZIF-67 (2 mg/L and 10 mg/L) and fixed concentrations of BPs are shown in Fig. 1. The LIRs of BPA and ZIF-67 were 37.9 % and 40.8 % at concentrations of 25 mg/L and 2 mg/L, respectively. The LIR of the mixture of BPA and ZIF-67 was 55.5 %, significantly higher than that of a single compound. BPA (25 mg/L) mixed with higher concentrations of ZIF-67 (10 mg/L) showed synergistic effects, with the LIR was 99.33 %. Similarly, the same trend was found in the mixed group of BPS and ZIF-67, the combined toxicity of the mixture was higher than that of the single compound ($p < 0.01$). The results of BPAF and ZIF-67 differ from those of the binary mixture mentioned above. The LIRs of BPAF (1 mg/L) and ZIF-67 (2 mg/L) are 35.1 % and 40.8 %, respectively, while the LIR of the mixture is 26.3 %, the combined toxicity is lower than that of the single compound, showing antagonism effect. When the test concentration of ZIF-67 increased to 10 mg/L, the LIR was 76.7 %, and that of the 1 BPAF-10

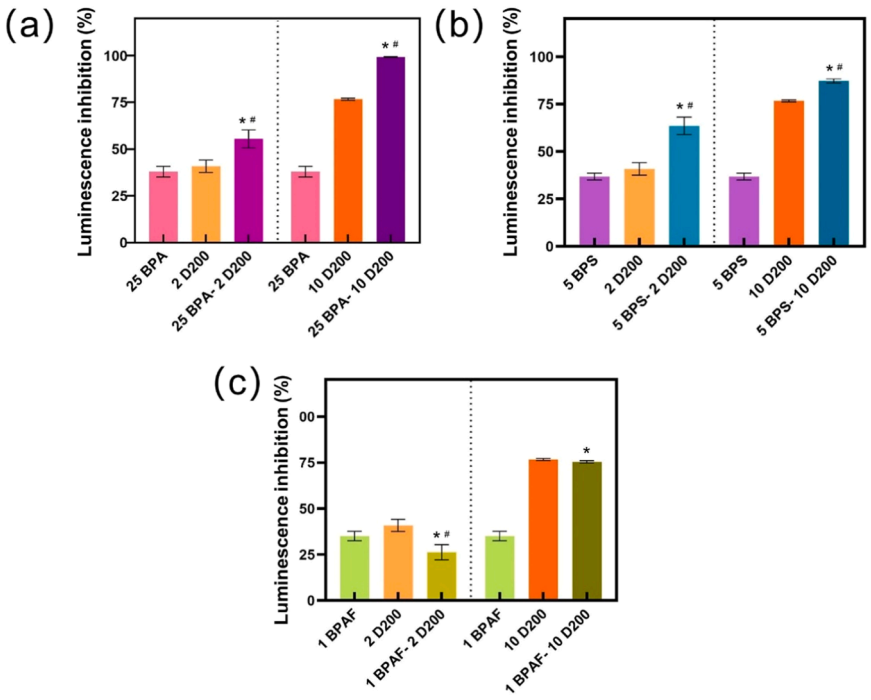

Fig. 1. Cytotoxicity of single and binary mixed group on T3 strain. (a)single and binary mixed toxicity of ZIF-67 and BPA, (b) single and binary mixed toxicity of ZIF-67 and BPS, (c) single and binary mixed toxicity of ZIF-67 and BPAF. (* $p < 0.01$ is compared with control, #$p < 0.01$ is compared withBPs group).

D200 group was 75.4 %, which was considered to be equivalent to the LIR of ZIF-67 (10 mg/L). The results showed that the toxicity effect of ZIF-67 and BPs were not the same, the combined effect of ZIF-67 and BPA, ZIF-67 and BPS showed mainly synergistic, while the ZIF-67 and BPAF were primarily antagonistic. Chen et al. found the antagonistic effect was the main effect in the Zn-based nanomaterials (ZnO-NPs and ZIF-8) on Cd^{2+} The high concentration of Zn-based nanomaterials (16 mg/L) and Cd^{2+} co-exposed to Cd^{2+} decreased bacterial activity and increased toxicity. However, co-exposure of Zn-based nanomaterials at a low concentration (4 mg/L) with Cd^{2+} resulted in detoxification and reduced toxicity [31].

3.3. Intracellular adsorption and distribution of ZIF-67 and BPs after co-exposure

3.3.1. Adsorption capacity of BPs on ZIF-67

The adsorption rate represented the percentage of the content of BPs adsorbed by ZIF-67 at fixed concentrations (Fig. 2). ZIF-67 had the lowest adsorption capacity for BPA, the adsorption rates of 2 mg/L and 10 mg/L ZIF-67 for 25 mg/L BPA were 8.68 % and 7.45 % respectively, which were lower than 10 %. The adsorption rate of ZIF-67 (2 mg/L) on BPS (5 mg/L) reaches 56.67 %, and the adsorption rate increased when the concentration of ZIF-67 increased. Among the three BPs, ZIF-67 adsorbed the largest amount of BPAF, with the adsorption rate of 1 mg/L of BPAF by 2 mg/L of ZIF-67 reaching 81.67 %, and the adsorption rate increased to 83.71 % at 10 mg/L of ZIF-67. As can be seen, the adsorption capacity of ZIF-67 for BPA, BPS and BPAF was different within 15 min. The adsorption capacity of ZIF-67 for BPAF reached 80 %, followed by BPS, and BPA was the lowest, with an adsorption rate of less than 10 %. Other researchers have also reported that the same material's adsorption ability for different BPs differs. Li et al. synthesized a magnetic layered bilge-shaped adsorbent (Fe_3O_4 @Co/Ni-LDH), which can adsorb BPA, BPS and BPAF at pH 7. The core-shell adsorbent has the best adsorption capacity for BPAF. It is also considered that high pH and salinity are unfavorable to removing BPs [32].

In order to further investigate the adsorption properties of ZIF-67 for three BPs, the adsorption mechanism was clarified by DFT (Fig. 3). It is showed that when the ZIF-67 configuration is fixed, the cobalt ion forms an electrostatic interaction with the benzene ring of BPA, an imidazole ring and a benzene ring can form an incomplete π-π stacking interaction, while the methyl group in BPA cannot participate in the interaction between the two molecules due to steric hindrance effect. The π-π stacking of the imidazole ring and benzene ring is dominant between BPS and ZIF-67, the interaction between cobalt and benzene ring is weak, while the sulfhydryl group in BPS formed a certain van der Waals force with cobalt ion due to strong electronegativity. BPAF has the fluorine-containing group with the strongest electronegativity, fluorine element and cobalt ion, forming the strong van der Waals force among the three BPs. In addition, cobalt interacted with benzene ring positively in the opposite direction. According to the diagram of interaction

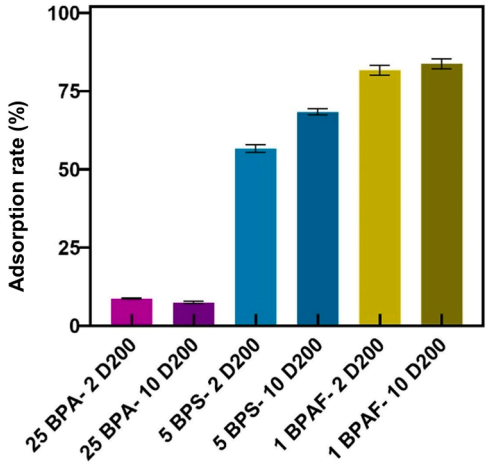

Fig. 2. Adsorption rate of ZIF-67 and bisphenol compounds. The initial concentrations of ZIF-67 were fixed at 2 and 10 mg/L, and the concentrations of BPA, BPS and BPAF were fixed at 25, 5and 1 mg/L, respectively. The initial pH was 6.5 and the temperature was 25 ℃.

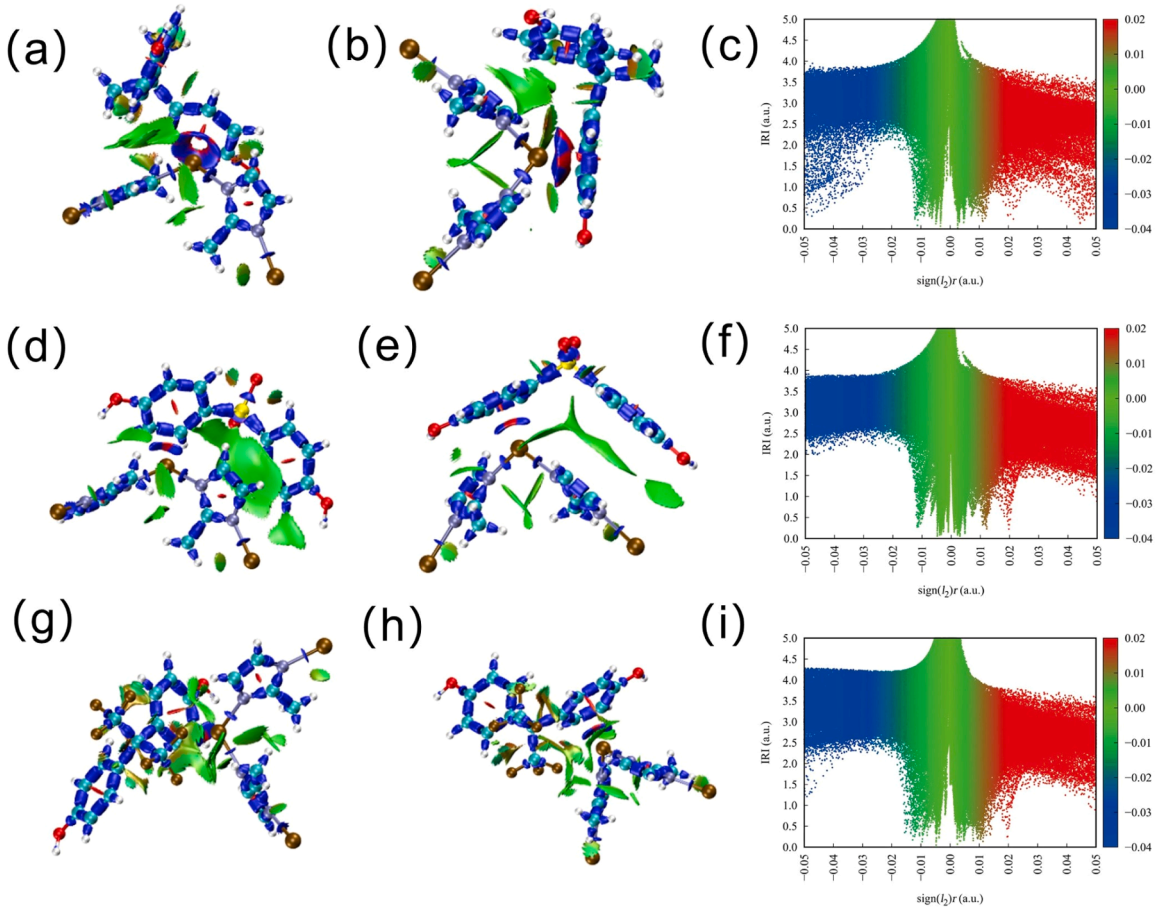

Fig. 3. DFT calculation results. Front view of (a) ZIF-67 and BPA, (d) ZIF-67 and BPS, and (j) ZIF-67 and BPAF, side view of (b) ZIF-67 and BPA, (e) ZIF-67 and BPS, and (h) ZIF-67 and BPAF. The weak interaction between ZIF-67 and BPs was reflected by the interaction region indicator (IRI), (c) the IRI of ZIF-67 and BPA, (f) the IRI of ZIF-67 and BPS, and (i) the IRI of ZIF-67 and BPAF.

strength, it can be determined that the interaction between BPAF and ZIF-67 is the strongest, followed by BPS and ZIF-67, and the interaction between BPA and ZIF-67 is the weakest. This result is in agreement with the analysis of the maximum site resistance induced by the two methyl groups and the maximum interaction force of fluorine. The DFT results are in concordance with the results of the adsorption tests.

3.3.2. Adsorption of BPs by intracellular ZIF-67

3.3.2.1. No difference in particle size between treatment groups after co-exposure. Studies related to the effect of particle size on the toxicity of nanomaterials have confirmed that particle size is one of the important factors affecting the toxicity of nanomaterials [33-35]. Therefore, the particle size variation after adsorption of ZIF-67 and BPs was investigated. In order to avoid agglomeration of nanomaterials at high concentrations, a low concentration of ZIF-67 (2 mg/L) was selected to investigate the change in particle size after the adsorption of BPs (Fig. S2). It can be found that the particle size distribution of BPA and ZIF-67 group is 140 nm, that of BPS and ZIF-67 group is 145 nm, and that of BPAF and ZIF-67 is 156 nm, indicating that there is no significant change in the particle size after the adsorption of ZIF-67 with the three BPs.

Previous studies have suggested that ZIF-67 with a particle size of less than 400 nm may enter the cell and cause biotoxicity [26]. Combined with this conclusion, it is assumed that the particle size of ZIF-67 adsorbed to BPs is less than 200 nm, which may enter the cells and cause toxic effects. Therefore, the intracellular levels of ZIF-67 and BPs after co-exposure were determined.

3.3.2.2. Determination and isolation of intracellular components. After the separation of ZIF-67 and BPs with dilute nitric acid, the content of intracellular BPs, the content of BPs adsorbed by intracellular ZIF-67, and the content of intracellular cobalt contained in the cells were determined by HPLC-MS, are shown in Table 1.

The content of intracellular BPs varied inT3 after 15 min of exposure, with the BPAF having a higher content of 29.12 %, followed by BPA (18.11 %) and BPS (15.07 %), indicating that the three BPs have different ability to enter the cell. The BPs reduced the firmness and hardness of monolayers, weakening the interaction between membrane-forming molecules [36]. The strength of action of BPA on cell membranes is greater than that of BPS, and it was speculated that BPA tends to aggregate into clusters at high concentrations, leading to the extraction of lipids from the bilayer and the eventual formation of voids, which caused cell membrane damage [37].

Our previous studies have demonstrated that the intracellular cobalt content after 15 min of treatment can reflect the amount of ZIF-67 entering the cell [26]. As shown in Table 1, the intracellular cobalt content after ZIF-67 (2 mg/L) treatment was 85.2 %, while the intracellular cobalt content of ZIF-67 mixed with BPs group decreased. The intracellular cobalt content was 47–52 % after mixing 2 mg/L of ZIF-67 with BPs, whereas the intracellular cobalt content decreased after combining ZIF-67 with BPs at a high concentration (10 mg/L). There was no significant difference in the percentage of cobalt content in the high-concentration ZIF-67 mixed with BPs, which was about 20–21 %. It is speculated that agglomerates of ZIF-67 in high concentrations are more difficult to enter cells [38].

Although the percentage of intracellular cobalt content in high-

Table 1
Determination of intracellular components.

Group	Intracellular free BPs		Intracellular BPs adsorbed by ZIF-67		Intracellular Co	
	Content (fg per cell)	Proportion (wt%)	Content (fg per cell)	Proportion (wt%)	Content (fg per cell)	Proportion (wt%)
2 D200	-	-	-	-	75.24 ± 6.42	85.2 ± 3.05
10 D200	-	-	-	-	215.4 ± 9.18	46.7 ± 1.08
25 BPA	20.65 ± 0.87	18.11 ± 2.38	-	-	-	-
5 BPS	3.75 ± 0.31	15.07 ± 1.47	-	-	-	-
1 BPAF	1.46 ± 0.66	29.12 ± 1.57	-	-	-	-
25 BPA−2 D200	1.86 ± 0.51	2.38 ± 0.26	5.18 ± 0.43	4.04 ± 0.43	52.18 ± 6.42	51.20 ± 2.11
25 BPA−10 D200	10.67 ± 0.72	8.47 ± 0.27	24.15 ± 0.93	19.18 ± 0.72	96.74 ± 5.91	20.97 ± 1.53
5 BPS−2 D200	0.34 ± 0.07	1.57 ± 0.14	1.32 ± 0.08	6.09 ± 0.34	53.18 ± 2.07	47.53 ± 1.37
5 BPS−10 D200	1.57 ± 0.40	7.26 ± 0.31	5.17 ± 0.42	23.85 ± 0.75	95.08 ± 3.39	20.26 ± 0.92
1 BPAF −2 D200	0.01 ± 0.01	0.27 ± 0.01	0.41 ± 0.21	8.11 ± 0.40	54.31 ± 8.10	51.58 ± 1.18
1 BPAF −10 D200	0.22 ± 0.04	4.39 ± 0.82	2.63 ± 0.58	52.02 ± 0.23	97.22 ± 4.90	21.53 ± 0.21

concentration ZIF-67mixed groups was lower than in the low-concentration group, the absolute amount of intracellular cobalt content increased, suggesting that co-exposure to high concentrations of ZIF-67 and BPs increases the ability of ZIF-67 to enter cells. The above results showed that the ability of ZIF-67 to enter the cell after co-exposure with three BPs was decreased compared to the ability of a single ZIF-67 to enter the cell, suggesting that ZIF-67 adsorbed with BPs is less likely to enter the cell and cause accumulation. However, there was no significant change in the ability of ZIF-67 to enter cells between the binary mixed groups, and this result is consistent with the fact that there was no significant difference in the change in particle size after co-exposure of ZIF-67 with three BPs. Although there was no significant difference in intracellular cobalt content in the binary mixed group at the same ZIF-67 concentration, the intracellular content of BPs was not the same due to the different adsorption capacities of ZIF-67 on the three BPs, and the intracellular BPs content increased with the increase of ZIF-67 concentration.

Compared with the BPA-D200 and BPS-D200 groups, the BPAF-D200 group had the highest BPAF adsorbed into the cell by ZIF-67. In the 25 BPA-2 D200 group, the percentage of BPA content adsorbed to ZIF-67 co-entering the cell was 4.04 %, and the intracellular free BPA content was 2.38 %. In the 25 BPA-10 D200 group, the BPA adsorbed to ZIF-67 co-entering the cell was 19.18 %, and the intracellular free BPA content was 8.47 %. Differently, in the 25 BPAF-2 D200 group, the percentage of BPAF adsorbed to ZIF-67 co-entering into the cell was 8.11 %; with the increase of ZIF-67 concentration to 10 mg/L, the content of BPS adsorbed to ZIF-67 co-entering the intracellular increased to 52.02 %. The adsorption capacity of ZIF-67 on BPA was weaker, the content of BPA in the cell after adsorption was lower, and the content of free BPA in the cell was higher. ZIF-67 had the strongest adsorption capacity on BPAF, which caused the content of intracellular BPAF to be lower than that of BPA and BPS. After adsorption of the three BPs, the intracellular content of free BPs was in the order of BPA > BPS > BPAF. Presumably, in the binary mixing group with low concentrations of ZIF-67, the ability of ZIF-67 to enter the cell is decreased when adsorbed with BPs. In the mixing group with a high concentration of ZIF-67, the ability of ZIF-67 to enter the cell was increased, probably because the high concentration of ZIF-67 caused more severe membrane damage. The intracellular adsorption experiments showed that in the mixed group with a low concentration of ZIF-67, the content of BPAF adsorbed by ZIF-67 was higher in the mixed group of BPAF-D200 compared to that of BPA-D200 and BPS-D200. The intracellular content of free BPs, showed the order of BPA > BPS > BPAF, it is speculated that free BPs may contribute to toxicity. Due to the technical limitations, there are no direct methods to demonstrate the process by which ZIF-67 entered the cell. With the help of TEM, we explored the intracellular distribution of the after the co-exposure of ZIF-67 and three BPs (Fig. S3). Bacteria in the control were round or oval-shaped, with no accumulation of exogenous material in the cell with clear cell membranes. In treatment groups, ZIF-67 could be seen interacting with the membrane, and some of the membranes appeared to be wrinkled, and nanomaterials accumulated in the cell. This result supports the speculation that ZIF-67 adsorbed BPs and co-entered the cell.

3.3.2.3. Toxicity contribution analysis. To further clarify the toxicity contribution, the LIRs of each component were converted based on the concentration-effect relation and the data in Table 1 (Fig. 4a). The toxicity contribution of ZIF-67 was much greater than that of free intracellular BPs, showed a higher toxicity contribution. The predicted LIR of intracellular BPs was higher in the mixed groups ofBPA-D200 and BPS-D200 than in the BPAF-D200 group, with the predicted LIR of BPs in the 25 BPA-2 D200 group being 6.47 %, and being as high as 18.14 % in the 25 BPA-10 D200 group. The predicted LIR of free intracellular BPs in the BPAF-D200 mixed group were all lower than 0.001 %, which can be considered no toxicological contribution. This result further supports the conclusion that the high adsorption capacity of ZIF-67 for BPAF leads to a decrease in the intracellular free BPAF content and a lower contribution to combined toxicity.

From the factor correlation analysis in Fig. 4b, the four factors, the intracellular BPs content, intracellular ZIF-67 adsorbed BPs content, intracellular ZIF-67 content and LIR showed a strong positive correlation. It can be concluded that the combined toxicity of BPs and ZIF-67 is not caused by the single component, which is the result of the individual action of the components and interaction.

3.4. The toxicity mechanism of ZIF-67 co-exposure to BPs

3.4.1. Cell membranes damage after co-exposure

The analysis of the percentage of live and dead bacteria in the single and mixed groups are shown in Fig. 5. The percentage of dead bacteria in the control was 4.89 % and the live bacteria was 93.73 %. The percentage of dead bacteria for three BPs, BPA (25 mg/L), BPS (5 mg/L), BPAF (1 mg/L), were 15.23 %, 10.94 %, and 10.40 %, respectively. The percentage of dead bacteria for 2 mg/L of ZIF-67 was 8.42 %, and that for 10 mg/L of ZIF-67 was 24.85 %. In the binary mixture group, the percentage of dead bacteria in the 25 BPA-2 D200 was 22.18 %, which was significantly higher than that of the single compounds of the two, indicating that the mixture of BPA and ZIF-67 caused cell membrane damage, which resulted in a significant increase in the number of dead bacteria, and showed synergistic effects. The same trend was observed as the concentration of ZIF-67 in the mixed group was increased to 10 mg/L. Similarly, the BPS-D200 mixture group showed a trend of a higher percentage of dead cells in the binary mixture group than that of the single compound, in which the percentage of dead bacteria in the 5 BPS −2 D200 group was 20.95 %, the percentage of dead bacteria in the 5 BPS and 2 D200 were 10.94 % and 8.42 %, respectively, showing synergistic effect. The results of the mixed group of BPAF and ZIF-67 were different from the above test groups. The percentage of dead bacteria in the 1 BPAF-2 D200 group was 5.71 %, which was much lower than the number of dead bacteria in the single compounds of the two (10.40 %

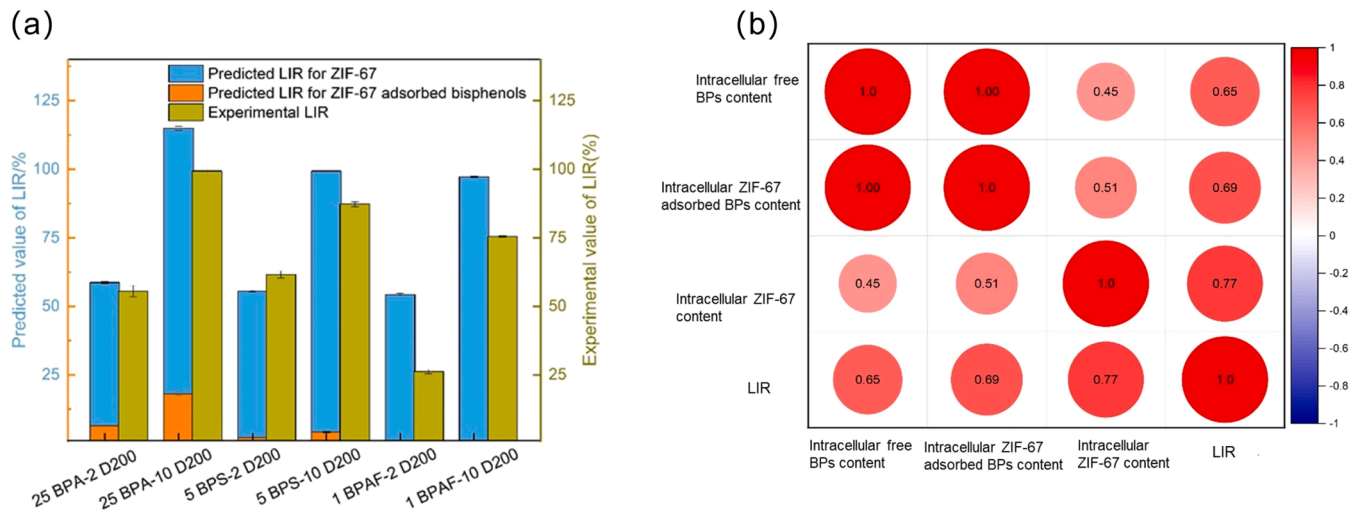

Fig. 4. (a) Percentage columnar plots of the toxicity contribution of ZIF-67 and ZIF-67 absorbed bisphenol compounds. (b) correlation analysis of bisphenol content, bisphenol content adsorbed by ZIF-67, intracellular ZIF-67 and LIR.

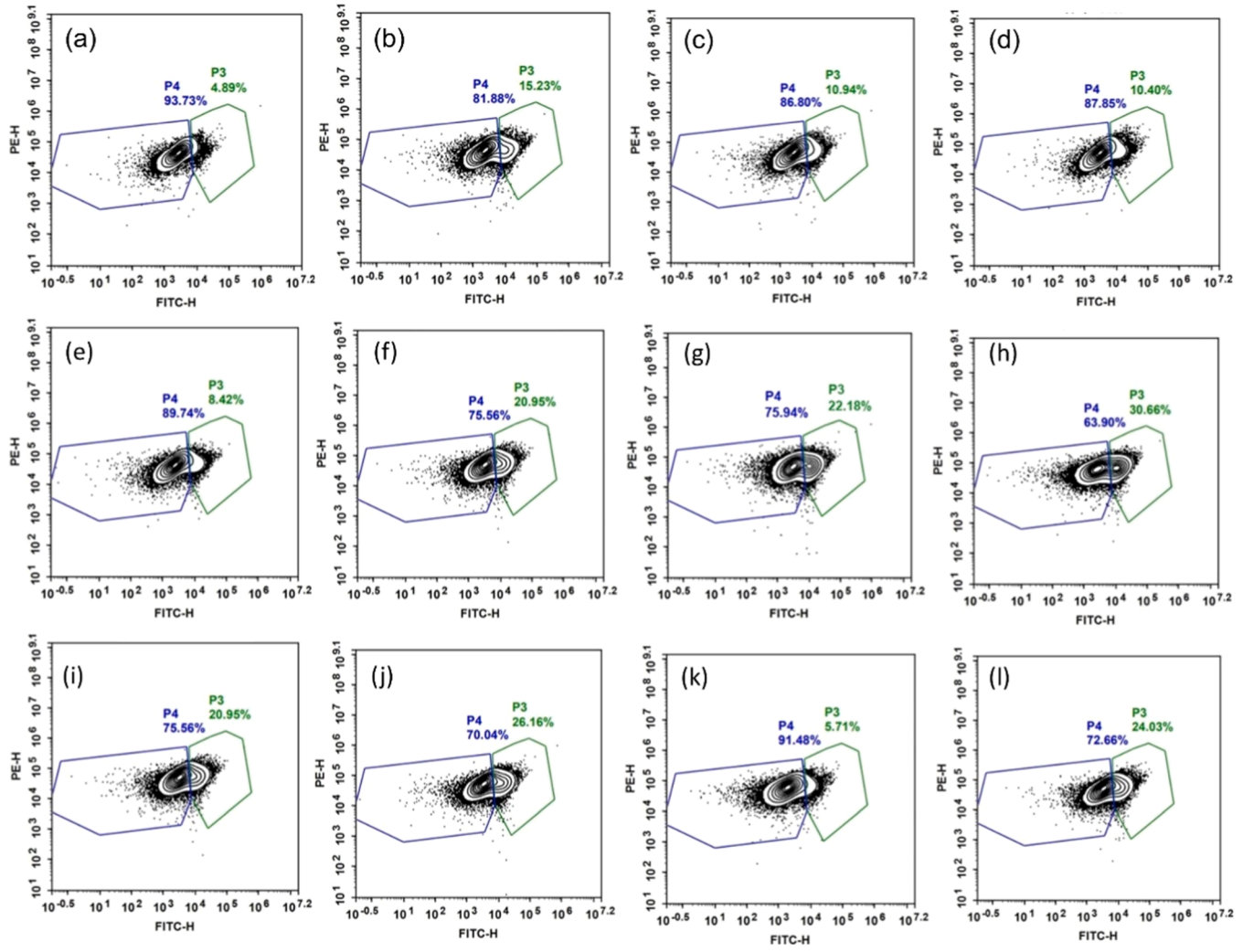

Fig. 5. Flow cytometry analysis for cells. (a) Control, (b) 25 BPA group, (c) 5 BPS group, (d) 1 BPA group, (e) 2 D200 group, (f) 10 D200 group, (g) 25 BPA −2 D200 group, (h) 25 BPA −10 D200 group, (i) 5 BPS −2 D200 group, (j) 5 BPS −10 D200 group, (k) 1 BPAF −2 D200 group, and (l) 1 BPAF −10 D200 group.

and 8.42 %, respectively), suggesting that the mixture would reduce the damage to the cell membrane, which showed the antagonistic effect. When the concentration of ZIF-67 in the mixed group was increased to 10 mg/L, the percentage of dead bacteria in the 1 BPAF-10 D200 group gradually increased to 24.03 %, the percentage of dead bacteria in the mixed group was still relatively low compared with that in the 5 BPA −10 D200 and 5 BPS −10 D200 groups.

The above results of the live/dead bacterial percentage of ZIF-67 and the three BPs indicate that cell membrane damage correlates with toxicity, the more severe the cell membrane damage, the greater the toxicity. Moreover, the cell membrane damage in the mixed group with a high concentration of ZIF-67 (10 mg/L) was more severe compared to that in the mixed group with a low concentration of ZIF-67 (2 mg/L), which verified the speculation above that the high concentration of ZIF-67 is prone to aggregation, and thus may produce more significant damage to the cell membrane.

3.4.2. *Oxidative damage analysis*

Oxidative damage in the combined group was explored using four indicators: intracellular ROS content, GSH content, total antioxidant activity and LDH activity. Due to the high toxicity of 10 mg/L of ZIF-67, which tends to contribute too much to the combined toxicity and neglect the toxicity contribution of BPs, 2 mg/L was chosen as the concentration of ZIF-67 in the mixture to investigate the oxidative damage.

Under the normal natural state of cells, ROS are natural by-products of oxygenation during normal metabolism, and intracellular oxidation reactions are in dynamic balance. However, external stimuli interfering with cellular structure and function can cause a dramatic rise in intracellular ROS, undesirable ROS becoming a product and triggering toxic effects [39]. As seen in Fig. 6a, the ROS content of T3 strain after 15 min exposure to 2 % DMSO was employed as a control of 60 U/mL. The ROS contents in all test groups were significantly higher than in control ($p < 0.01$). The ROS content in the BPA and ZIF-67 was 145 and 158 U/mL, while the ROS content in the mixed group was 232 U/mL, which was 37.5 % and 31.9 % higher compared with the ROS generation of the two single components. Similarly, the single ROS generation of 5 mg/L of BPS and 2 mg/L of ZIF-67 was 113 and 158 U/mL, respectively, whereas that of the combined group of the two was 184 U/mL, which was higher than the ROS content produced by BPS and ZIF-67 single component ($p < 0.01$). Although the ROS content of the mixed test group was higher than that of the single component, it was still lower than that of the single component summed ROS content. Combined with the adsorption results, this may be due to the strong adsorption capacity of ZIF-67 on BPA and BPS, which led to the reduction of the free BPA and BPS that entered into the intracellular through the cell membrane, which was finally manifested as the ROS generation of the mixed group was lower than that of the single component summed ROS generation.

In contrast to the results of these two mixed groups, the ROS generation of 105 U/mL in the mixed group of BPAF and ZIF-67 was significantly higher than that of the single component ($p < 0.01$). The decrease in ROS generation indicates a reduction in intracellular oxidative stress compared to the single component. The results suggest that the ROS content is correlated with the combined toxicity. When the combined toxicity was synergistic, the ROS content of the mixed group was higher than that of the single-component group. When the combined toxicity was antagonistic, the ROS content of the mixed group was lower than that of the single-component group.

Several studies have shown that ROS generation is accompanied by intracellular detoxification. Glutathione (GSH), which consists of glutamate, cysteine and glycine, as an essential regulator of metabolism, will participate in the tricarboxylic acid cycle and glucose metabolism pathways in vivo to promote metabolism and is an important detoxifying agent [40-42]. Therefore, changes in GSH content reflect the

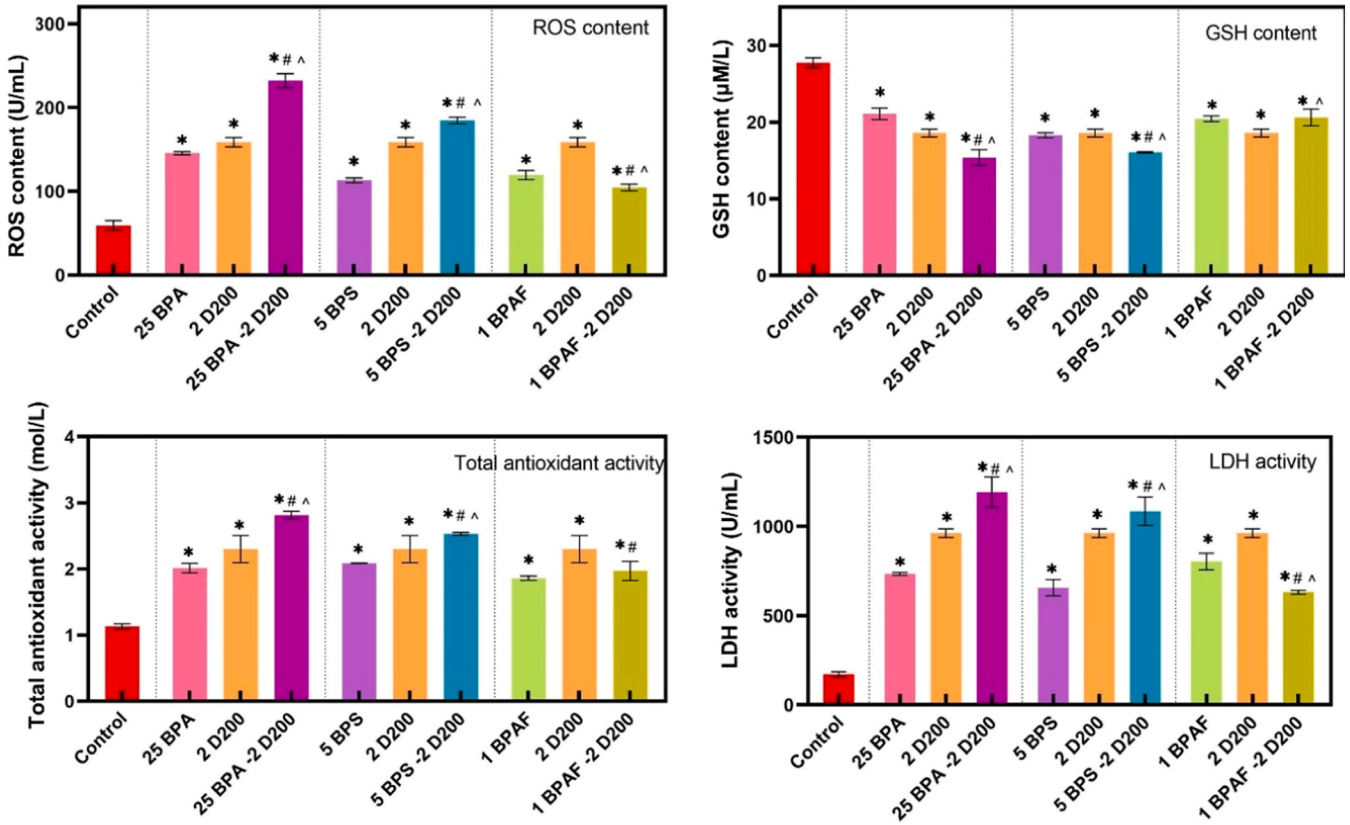

Fig. 6. Oxidative damage investigation in single and binary mixtures of ZIF-67 and BPs. (a) ROS content, (b) GSH content, (c) Total antioxidant activity and (d) LDH activity. (* $p < 0.01$ compared with the control, #$p < 0.01$ compared with the BP in the group, ^$p < 0.01$ compared with the ZIF-67).

degree of intracellular oxidative stress [14]. All treatment groups showed a significant decrease in GSH content compared to the control ($p < 0.01$). As shown in Fig. 6b, the mixture group of ZIF-67 and BPA/BPS showed similar results, with significantly lower GSH content in the mixture group compared to the single component ($p < 0.01$). However, the GSH content of the BPAF and ZIF-67 mixture group did not show a significant reduction ($p > 0.01$) compared to that of the two components, where the GSH content of the single-component BPAF (1 mg/L) experimental group was about 20.4 μM/L and that of the other components, ZIF-67 (2 mg/L), was about 18.6 μM/L. The GSH content of the mixed group was about 20.7 μM/L, which was slightly higher than that of the single component. The results indicated that the intracellular production of ROS was lower in the BPAF-D200 mixed group, which resulted in higher intracellular GSH content. The results of GSH content indicated that GSH was involved in the detoxification mechanism of intracellular oxidative stress. The balance of ROS and GSH is required to clear the normal physiological activities, and redox homeostasis is maintained through the production of GSH. The disruption of the balance of ROS/GSH will destroy the ROS/GSH homeostasis. Disruption of the GSH balance leads to undesirable oxidation and chemical modification of biomolecules, resulting in cell cycle arrest, inhibition of proliferation, and ultimately inducing cell death. It has been suggested that the imbalance of intracellular ROS and GSH can regulate cell proliferation, differentiation, and death through specific signal pathways [43,44].

The change in total antioxidant activity (T-AOC) is a more intuitive indication of the level of intracellular oxidative stress. When intracellular oxidized free radicals accumulate, the activity of antioxidant enzymes will be significantly elevated, using redox to convert peroxides into less toxic or harmless substances, reducing the level of intracellular oxidative stress and decreasing the toxicity [45-47]. As shown in Fig. 6c, T-AOC was increased in all test groups compared to the control group ($p < 0.01$). The most significant increase in T-AOC compared to a single component was in the mixed group of ZIF-67 and BPA, followed by the mixed group of ZIF-67 and BPS. The trend of change was different is the BPAF and ZIF-67 test group, and there was a slight increase in T-AOC in the mixed group compared to the T-AOC of the component BPAF (1 mg/L) and a 17 % decrease in T-AOC compared to that of the component ZIF-67 (2 mg/L) ($p > 0.01$). Combined with the results of GSH content and T-AOC measurements, it indicated that the level of oxidative stress was lower in the mixed group of BPAF and D200, and thus it can be assumed that intracellular oxidative stress is one of the reasons for the toxicity.

LDH activity can characterize the extent of membrane damage [48], and the results are shown in Fig. 6d. LDH activity was significantly increased in all tested groups compared to the control ($p < 0.01$). The most highly increased of the mixed groups was the BPA-D200 mixture group, which showed a 62.8 % increase in LDH activity over the component BPA group (10 mg/L) and a 24 % increase over ZIF-67 (2 mg/L). Similarly, LDH activity was elevated in the BPS-D200 mixed group compared to the single component. The reduced LDH activity in the mixed group was in the BPAF-D200 group, with a measured LDH activity of 632.8 mU/mL in the mixed group, which was significantly lower compared with the LDH activities of component BPAF (1 mg/L) and component ZIF-67 (2 mg/L), 803.9 and 962.8 mU/mL, which were consistent with the results measured by flow cytometry, suggesting that the mixed group of BPAF and D200 showed reduced damage to the cell membrane compared to the single component. The above results are consistent with the results measured by flow cytometry, indicating that the degree of damage decreased in the BPAF -D200 group and increased in the BPAF -D200 and BPS-D200 mixed group. Considering the results that the levels of intracellular ZIF-67 and intracellular ZIF-67 adsorbed BPAF were low compared to the remaining two groups, it is assumed that the ability of ZIF-67 and BPAF to enter the cell after co-exposure was reduced, resulting in less damage to the cell membrane. It has been suggested that cell membranes contain a lipid bilayer that is susceptible to ROS attack. ROS activate oxidative stress, leading to lipid peroxidation and cell membrane damage. Cell membrane damage causes more extensive damage to the cell, ultimately leading to cell death [49]. In addition, we speculate that excess nanomaterial is attached to the cell membrane, interfering with the normal function of ion channels in the membrane and causing cell membrane damage [50].

The results of the above measurements of intracellular ROS content, GSH content, T-AOC and LDH activity indicated that the mixed groups of ZIF-67 and BPA, and ZIF-67 and BPS induced a dramatic increase in ROS, which led to a decrease in intracellular GSH and an increase in the activity of total antioxidant enzymes in response to oxidative damage.

3.4.3. Luminescence damage analysis

The FMN content, NADH content, and the relative expression of mRNAs encoding *lux*A and *lux*B were used to analyze the luminescence damage caused by ZIF-67 and BPs on T3 strain.

3.4.3.1. FMN content. FMN (Flavin mononucleotide) is a cofactor of flavin protein and can play an important role in electron transfer during luminescence [51,52]. As shown in Fig. 7a, all test groups showed a significant reduction in FMN content compared to the control group ($p < 0.01$). The highest decrease was observed in the BPA-D200 group, with a 64 % reduction compared to the control. The FMN content of this mixed group was also significantly lower than that of the single components BPA and ZIF-67, with the FMN content of BPA (25 mg/L) being 145.5 ng/mL and that of ZIF-67 (2 mg/L) being 129.0 ng/mL. The FMN content of the ZIF-67 and BPS mixed group was significantly lower ($p < 0.01$) than that of the single components ZIF-67 and BPS. There was no significant change in the FMN content of the components ZIF-67 and BPS, FMN content of the mixed test group of ZIF-67 and BPAF was increased compared to that of the single components ZIF-67 and BPAF ($p < 0.01$). Fig. 8.

3.4.3.2. NADH content. NADH and NAD^+ act as a redox pair in the cell, with NADH acting as a hydrogen and electron donor and NAD^+ acceptor involved in various redox reactions [53]. As seen in Fig. 7b, compared to the control, all test groups showed a significant decrease in NADH content ($p < 0.01$). The most significant decrease in NADH content was in the BPA-D200 group, which was reduced by 84 % compared to the control. Similarly, the NADH content of the BPS-D200 mixed group was also reduced compared to the single components BPS and ZIF-67. NADH content of the BPAF and D200 mixed groups did not change significantly compared to the single components.

Variations in the FMN and NADH contents of the mixed and single component test groups were generally consistent with the changes in toxicity. It has been reported that an imbalance in the ratio of NADH and NAD^+ produces ROS, and NADH and FMN are two critical energetic substrates. More studies have been conducted on FMN and NADH content to characterize the toxicity mechanism. It was found that while 1-alkyl-3-methylimidazoles had a toxic stimulatory effect on luminescent bacteria, the compounds greatly stimulated the production of FMN and NADH, suggesting that the stimulation of luminescence may be accompanied by an increase in the content of FMN and NADH [54]. By exploring the effect of carbon nanomaterials on the coupled enzyme system of luminescent bacteria: NAD(P)H:FMN-oxidoreductase and luciferase, Esimbekova et al. found that the soluble coupled enzyme system showed high sensitivity to MWCNT and SWCNT, and the inhibitory activity of carbon nanomaterial correlated with the toxicity of luminescent bacteria [55]. Mo et al. also used the FMN and NADH indicators to explore the time-dependent toxic stimulatory effects of four quinolone antibiotics, singly and in binary mixtures on *Vibrio qinghaiensissp*. Q67 [52].

3.4.3.3. Relative mRNA expression of core luminescent genes luxA and luxB. The expression of the core luminescent genes in the treatment

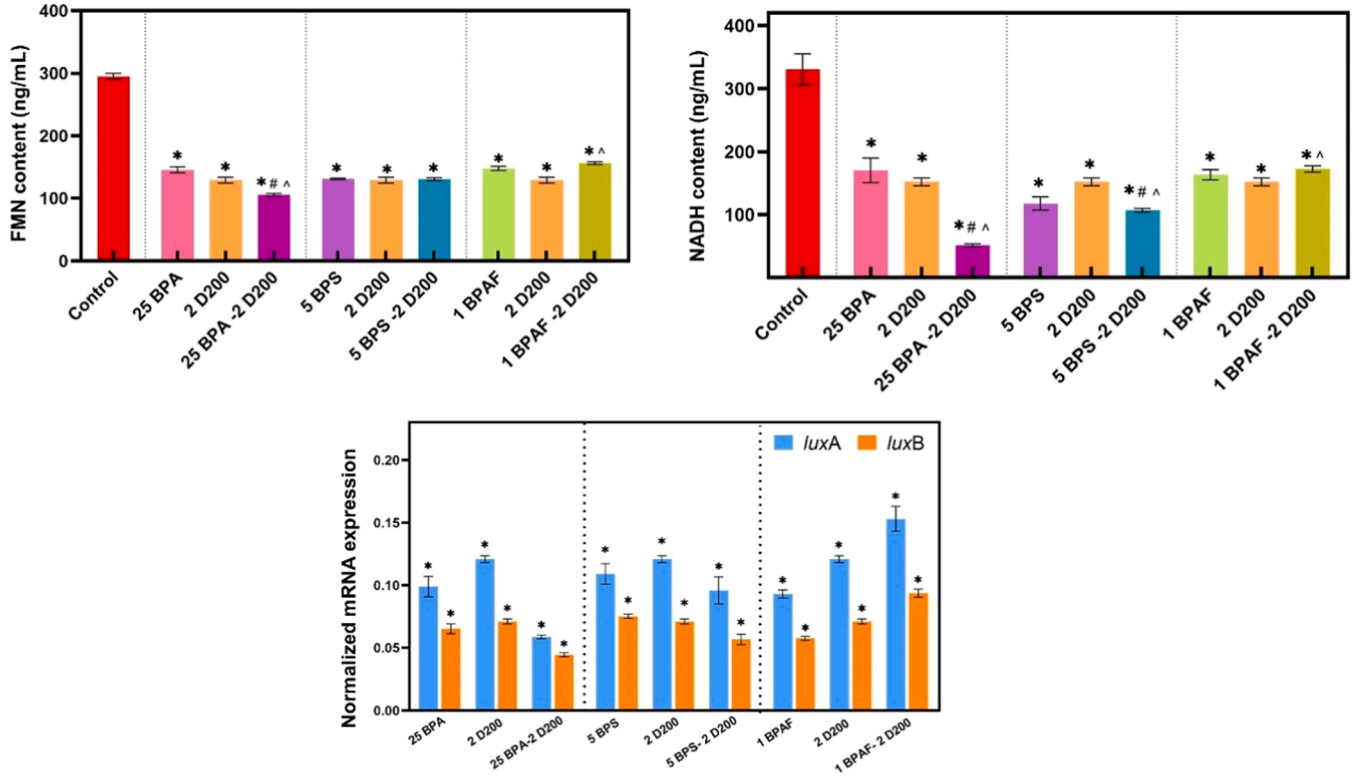

Fig. 7. Luminescence damage investigation in single and binary mixtures of ZIF-67 and BPs. (a) FMN content, (b) NADH content, (c) the mRNA expression of *lux*A and *lux*B. (* $p < 0.01$ compared with the control, #$p < 0.01$ compared with the BP in the group, ^$p < 0.01$ compared with the ZIF-67).

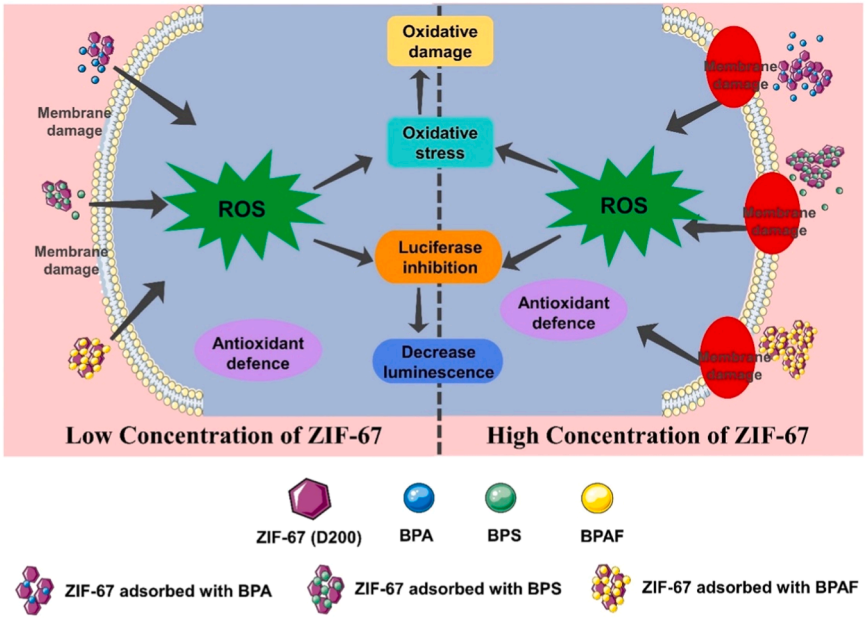

Fig. 8. Diagram of the potential toxicity of ZIF-67 and bisphenol compounds.

groups of ZIF-67 and BPs was explored by RT-PCR (Fig. 7c). The luminescent genes *lux*A and *lux*B are derived from the *lux* operon, which are two vital genes to encode luciferase and related to the luminescence intensity [56]. Mallevre et al. prepared a switch-off luminescent *Pseudomonas putida* BS566::luxCDABE bioreporter, which contained a complete *lux* operon from *Photorhabdus luminescens*, to investigate the toxicity effects of model OECD nanoparticles (Ag, ZnO and TiO_2). The results showed the toxicity results were associated with differences in agglomeration status and dissolution rate of nanoparticles [57]. The relative mRNA expression of *lux*A and *lux*B decreased in treatment groups. Compared to *lux*A, *lux*B has a significant decrease, indicating that *lux*B was more sensitive than *lux*A in response to external stress [58]. The lowest relative mRNA expression of *lux*A and *lux*B was in the BPA-D200 group, followed by the BPS-D200 group and BPAF-D200 group. The results were in good agreement with the toxicity results, indicating that all mixed groups inhibited the luminescence process by

inhibiting the expression of the core genes, leading to luminescence damage.

3.5. Potential toxicity mechanism

In this study, the combined toxicity of ZIF-67 and BPs (BPA, BPS, BPAF) was investigated, and the results showed that the different adsorption capacities of ZIF-67 on different BPs affected their combined toxicity effects. ZIF-67 had a stronger adsorption capacity for BPAF, and the co-exposure showed antagonistic effects; ZIF-67 showed weaker adsorption capacity for BPA and BPS, and combined toxicity showed synergistic effects, the potential toxicity mechanisms are shown in Fig. 6. At low concentrations of ZIF-67, the ability of ZIF-67 with adsorbed BPs to enter the cell was reduced, but still causing the cell membrane damage during the transmembrane process. In addition, due to the different adsorption capacities of ZIF-67 for BPs, the amount of free BPs detected in the cell showed an order of BPA > BPS > BPAF. In comparison, a smaller amount of free BPAF produced less ROS. Furthermore, the mutual repulsion of the most electronegative fluorine in BPAF and negatively charged cellular membrane also reduced cell membrane damage. The above reasons resulted in the antagonistic effect of co-exposure of BPAF and ZIF-67. At a high concentration, ZIF-67 aggregates caused large pores in the cell membrane, leading to more severe cell membrane damage while increasing the transmembrane capacity of ZIF-67 and BPs to enter the cell. The expression of luminescent genes *lux*A and *lux*B was inhibited, interfered with luciferase synthesis, and ultimately manifested as luminescence decrease.

4. Conclusion

In this study, the results of the acute toxicity assay of *Photobacterium phosphoreum* T3 showed that the combined toxicity of ZIF-67 and BPA, ZIF and BPS was mainly synergistic, the combined toxicity of ZIF-67 and BPAF was mainly antagonistic. In the mixed group of a low concentration of ZIF-67 and BPs, the ability of ZIF-67 adsorbed with BPs to enter the cell decreased compared to that of ZIF-67. Significant differences in the intracellular amount of BPs adsorbed by ZIF-67 due to differences in adsorption capacity led to significant differences in the intracellular amount of free BPs, which contributed to toxicity. There was no significant change in the particle size of ZIF-67 after the adsorption of different biphenolic compounds, and ZIF-67 acted as a transporter to carry the bisphenol compounds to enter the cell, causing oxidative damage and luminescence damage. Considerably more work need to be done to dynamically explore the interaction and intracellular entry of ZIF-67 and bisphenol compounds. These findings will contribute to more realistic environmental risk assessments of co-exposure to nanomaterials and other contaminants.

Environmental implication

Due to the adequate surface area and tunable surface chemistry, MOFs are considered a potential adsorbent widely used for the adsorptive removal of bisphenol compounds (BPs). The combined effects of typical zinc-based MOF (ZIF-67) and three BPs were investigated, and the adsorption properties of ZIF-67 on BPs were also explored, ultimately elucidating the mechanism of combined toxicity. This study provides new insights into the safety of MOF and other environmental contaminations and lays a theoretical foundation for the safe application and emission of nanomaterials.

CRediT authorship contribution statement

Wei Yan: Writing – review & editing, Supervision. **Wenlong Wang:** Writing – review & editing, Investigation. **Linming Bai:** Writing – review & editing, Investigation. **Shanshan LI:** Writing – review & editing, Supervision, Methodology, Funding acquisition. **Ruixue Zhang:** Writing – review & editing, Investigation. **Dan Wang:** Writing – review & editing, Writing – original draft, Methodology, Investigation, Conceptualization.

Declaration of Competing Interest

The authors declare that they have no known competing financial interests or personal relationships that could have appeared to influence the work reported in this paper.

Acknowledgements

This work was supported by the National Key R&D Program of China (Grant number 2019YFB2103003).

Appendix A. Supporting information

Supplementary data associated with this article can be found in the online version at doi:10.1016/j.jhazmat.2024.136140.

Data Availability

Data will be made available on request.

References

[1] Fonseca, J., Meng, L., Imaz, I., Maspoch, D., 2023. Self-assembly of colloidal metal-organic framework (MOF) particles. Chem Soc Rev 52 (7), 2528–2543.
[2] Huang, H., Li, J., Yuan, M., Yang, H., Zhao, Y., Ying, Y., et al., 2022. Large-scale self-assembly of mofs colloidosomes for bubble-propelled micromotors and stirring-free environmental remediation. Angew Chem-Int Ed 61 (46).
[3] Jiao, L., Seow, J.Y.R., Skinner, W.S., Wang, Z.U., Jiang, H.L., 2019. Metal-organic frameworks: structures and functional applications. Mater Today 27, 43–68.
[4] Wang, S., McGuirk, C.M., d'Aquino, A., Mason, J.A., Mirkin, C.A., 2018. Metal-organic framework nanoparticles. Adv Mater 30 (37).
[5] Ma, D., Huang, X., Zhang, Y., Wang, L., Wang, B., 2023. Metal -organic frameworks: synthetic methods for industrial production. Nano Res 16 (5), 7906–7925.
[6] Li, J., Wang, X., Zhao, G., Chen, C., Chai, Z., Alsaedi, A., et al., 2018. Metal-organic framework-based materials: superior adsorbents for the capture of toxic and radioactive metal ions. Chem Soc Rev 47 (7), 2322–2356.
[7] Rasheed, T., Hassan, A.A., Bilal, M., Hussain, T., Rizwan, K., 2020. Metal-organic frameworks based adsorbents: a review from removal perspective of various environmental contaminants from wastewater. Chemosphere 259.
[8] Zhao, X., Zheng, M., Gao, X., Zhang, J., Wang, E., Gao, Z., 2021. The application of MOFs-based materials for antibacterials adsorption. Coord Chem Rev 440.
[9] Ahsan, M.A., Jabbari, V., Islam, M.T., Turley, R.S., Dominguez, N., Kim, H., et al., 2019. Sustainable synthesis and remarkable adsorption capacity of MOF/graphene oxide and MOF/CNT based hybrid nanocomposites for the removal of Bisphenol A from water. Sci Total Environ 673, 306–317.
[10] Yu, K., Lee, Y.R., Seo, J.Y., Baek, K.Y., Chung, Y.M., Ahn, W.S., 2021. Sonochemical synthesis of Zr-based porphyrinic MOF-525 and MOF-545: enhancement in catalytic and adsorption properties. Microporous Mesoporous Mater 316.
[11] Arul, P., Huang, S.T., Gowthaman, N.S.K., Mani, G., Jeromiyas, N., Shankar, S., et al., 2021. Electrocatalyst based on Ni-MOF intercalated with amino acid-functionalized graphene nanoplatelets for the determination of endocrine disruptor bisphenol A. Anal Chim Acta 1150.
[12] Wan, Y., Zhang, W., Han, X., Zhou, L., Zhen, H., Wu, C., et al., 2022. B, N-decorated carbocatalyst based on Fe-MOF/BN as an efficient peroxymonosulfate activator for bisphenol A degradation. J Hazard Mater 430.
[13] Nunez, S.S., Ortuno, N., Fernandez-Duran, S., Molto, J., Conesa, J.A., 2024. Analysis and removal of bisphenols in recycled plastics using polyethylene glycol. Sci Rep 14 (1), 12824. -12824.
[14] Mao, J.F., Li, W., Ong, C.N., He, Y., Jong, M.C., Gin, K.Y.H., 2022. Assessment of human exposure to benzophenone-type UV filters: a review. Environ Int 167.
[15] Wu, L.H., Zhang, X.M., Wang, F., Gao, C.J., Chen, D., Palumbo, J.R., et al., 2018. Occurrence of bisphenol S in the environment and implications for human exposure: a short review. Sci Total Environ 615, 87–98.
[16] Kawa, I.A., Masood, A., Fatima, Q., Mir, S.A., Jeelani, H., Manzoor, S., et al., 2021. Endocrine disrupting chemical Bisphenol A and its potential effects on female health. Diabetes Metab Syndr-Clin Res Rev 15 (3), 803–811.
[17] Chen, M.Y., Ike, M., Fujita, M., 2002. Acute toxicity, mutagenicity, and estrogenicity of bisphenol-A and other bisphenols. Environ Toxicol 17 (1), 80–86.
[18] Helies-Toussaint, C., Peyre, L., Costanzo, C., Chagnon, M.C., Rahmani, R., 2014. Is bisphenol S a safe substitute for bisphenol A in terms of metabolic function? An in vitro study. Toxicol Appl Pharmacol 280 (2), 224–235.

[19] Qiu, W., Yang, M., Liu, J., Xu, H., Luo, S., Wong, M., et al., 2019. Bisphenol S-induced chronic inflammatory stress in liver via peroxisome proliferator-activated receptor γ using fish in vivo and in vitro models. Environ Pollut 246, 963–971.
[20] Qiu, W., Zhan, H., Hu, J., Zhang, T., Xu, H., Wong, M., et al., 2019. The occurrence, potential toxicity, and toxicity mechanism of bisphenol S, a substitute of bisphenol A: a critical review of recent progress. Ecotoxicol Environ Saf 173, 192–202.
[21] Liu, J., Wen, Y., Mo, Y., Liu, W., Yan, X., Zhou, H., et al., 2023. Chemical speciation determines combined cytotoxicity: examples of biochar and arsenic/chromium. J Hazard Mater 448.
[22] Wu, K., Li, Y., Zhou, Q., Hu, X., Ouyang, S., 2023. Integrating FTIR 2D correlation analyses, regular and omics analyses studies on the interaction and algal toxicity mechanisms between graphene oxide and cadmium. J Hazard Mater 443.
[23] Hu, X., Kang, J., Lu, K., Zhou, R., Mu, L., Zhou, Q., 2014. Graphene oxide amplifies the phytotoxicity of arsenic in wheat. Sci Rep 4, 6122.
[24] Gellert, G., 2000. Sensitivity and significance of luminescent bacteria in chronic toxicity testing based on growth and bioluminescence. Ecotoxicol Environ Saf 45 (1), 87–91.
[25] Steinberg, S.M., Poziomek, E.J., Engelmann, W.H., Rogers, K.R., 1995. A review of environmental applications of bioluminescence measurements. Chemosphere 30 (11), 2155–2197.
[26] Wang, D., Bai, L., Huang, X., Yan, W., Li, S., 2022. Size-dependent acute toxicity and oxidative damage caused by cobalt-based framework (ZIF-67) to *Photobacterium phosphoreum*. Sci Total Environ 851.
[27] Wang, D., Bai, L., Wang, W., Li, S., Yan, W., 2024. Functional groups effect on the toxicity of modified ZIF-90 to *Photobacterium phosphoreum*. Chemosphere 351, 141188. -141188.
[28] Brodl, E., Winkler, A., Macheroux, P., 2018. Molecular mechanisms of bacterial bioluminescence. Comput Struct Biotechnol J 16, 551–564.
[29] Tisler, T., Krel, A., Gerzelj, U., Erjavec, B., Dolenc, M.S., Pintar, A., 2016. Hazard identification and risk characterization of bisphenols A, F and AF to aquatic organisms. Environ Pollut 212, 472–479.
[30] Zhang, J., Zhang, T., Guan, T., Yu, H., Li, T., 2017. In vitro and in silico assessment of the structure-dependent binding of bisphenol analogues to glucocorticoid receptor. Anal Bioanal Chem 409 (8), 2239–2246.
[31] Chen, P., Chen, B., He, M., Hu, B., 2021. Combined effects of different sizes of ZnO and ZIF-8 nanoparticles co-exposure with Cd^{2+} on HepG2 cells. Sci Total Environ 786.
[32] Li, G., Zhang, X., Sun, J., Zhang, A., Liao, C., 2020. Effective removal of bisphenols from aqueous solution with magnetic hierarchical rattle-like Co/Ni-based LDH. J Hazard Mater 381.
[33] Gatoo, M.A., Naseem, S., Arfat, M.Y., Dar, A.M., Qasim, K., Zubair, S., 2014. Physicochemical properties of nanomaterials: implication in associated toxic manifestations. Biomed Res Int 2014.
[34] Sengul, A.B., Asmatulu, E., 2020. Toxicity of metal and metal oxide nanoparticles: a review. Environ Chem Lett 18 (5), 1659–1683.
[35] Yuan, X., Zhang, X., Sun, L., Wei, Y., Wei, X., 2019. Cellular toxicity and immunological effects of carbon-based nanomaterials. Part Fibre Toxicol 16.
[36] Hac-Wydro, K., Polec, K., Broniatowski, M., 2019. The comparative analysis of the effect of environmental toxicants: bisphenol A, S and F on model plant, fungi and bacteria membranes. The studies on multicomponent systems. J Mol Liq 289.
[37] Chen, L., Chen, J., Zhou, G., Wang, Y., Xu, C., Wang, X., 2016. Molecular dynamics simulations of the permeation of Bisphenol A and pore formation in a lipid membrane. Sci Rep 6.
[38] Murugadoss, S., Brassinne, F., Sebaihi, N., Petry, J., Cokic, S.M., Van Landuyt, K.L., et al., 2020. Agglomeration of titanium dioxide nanoparticles increases toxicological responses in vitro and in vivo. Part Fibre Toxicol 17 (1).
[39] Sies, H., Belousov, V.V., Chandel, N.S., Davies, M.J., Jones, D.P., Mann, G.E., et al., 2022. Defining roles of specific reactive oxygen species (ROS) in cell biology and physiology. Nat Rev Mol Cell Biol 23 (7), 499–515.
[40] Hu, J., Zhu, J., Wang, K., Yan, X., Xu, L., Zhang, X., et al., 2024. Engineered-doping strategy for self-sufficient reactive oxygen species blossom to amplify ferroptosis/cuproptosis sensibilization in hepatocellular carcinoma treatment. Adv Funct Mater.
[41] Lee, E.J., Jang, W.B., Choi, J., Lim, H.J., Park, S., Rethineswaran, V.K., et al., 2023. The protective role of glutathione against doxorubicin-induced cardiotoxicity in human cardiac progenitor cells. Int J Mol Sci 24 (15).
[42] Seydi, E., Rahemi, M., Esmaily, H., Arjmand, A., Pourahmad, J., 2023. Mitochondrial transplantation attenuates toxicity in rat renal proximal tubular cells caused by Favipiravir. J Pharm Pharmacol 75 (11), 1458–1466.
[43] Chowdhury, A.A., Chaudhuri, J., Biswas, N., Manna, A., Chatterjee, S., Mahato, S. K., et al., 2013. Synergistic apoptosis of CML cells by buthionine sulfoximine and hydroxychavicol correlates with activation of AIF and GSH-ROS-JNK-ERK-iNOS pathway. Plos One 8 (9).
[44] Liu, T., Sun, L., Zhang, Y., Wang, Y., Zheng, J., 2022. Imbalanced GSH/ROS and sequential cell death. J Biochem Mol Toxicol 36 (1).
[45] Fan, W., Wang, X., Cui, M., Zhang, D., Zhang, Y., Yu, T., et al., 2012. Differential oxidative stress of octahedral and cubic Cu2O micro/nanocrystals to *Daphnia magna*. Environ Sci Technol 46 (18), 10255–10262.
[46] Siqueira, P.R., Souza, J.P., Venturini, F.P., Carmo, T.L.L., Azevedo, V.C., Estevao, B.M., et al., 2023. rGO outperforms GO in generating oxidative stress and DNA strand breaks in zebrafish liver cells. Aquat Toxicol 262.
[47] Vineetha, V.P., Girija, S., Soumya, R.S., Raghu, K.G., 2014. Polyphenol-rich apple (Malus domestica L.) peel extract attenuates arsenic trioxide induced cardiotoxicity in H9c2 cells via its antioxidant activity. Food Funct 5 (3), 502–511.
[48] Kumar, P., Nagarajan, A., Uchil, P.D., 2018. Analysis of cell viability by the lactate dehydrogenase assay. Cold Spring Harb Protoc 2018 (6).
[49] Wang, Y., Ding, L., Yao, C., Li, C., Xing, X., Huang, Y., et al., 2017. Toxic effects of metal oxide nanoparticles and their underlying mechanisms. Sci China Mater 60, 93–108.
[50] Wang, Y., Yao, C., Li, C., Ding, L., Liu, J., Dong, P., et al., 2015. Excess titanium dioxide nanoparticle son the cell surface induce cytotoxicity by hindering ion exchange and disrupting exocytosis processes. Nanoscale 7, 13105–13115.
[51] Ma, X.Y., Wang, X.C., Huu Hao, N., Guo, W., Wu, M.N., Wang, N., 2014. Bioassay based luminescent bacteria: Interferences, improvements, and applications. Sci Total Environ 468, 1–11.
[52] Mo, L.Y., Wang, J., Qin, L.T., Yang, Y.L., Liang, N., 2023. Mechanism of time-dependent toxicity of quinolone antibiotics on luminescent bacteria *Vibrio qinghaiensis* sp.-Q67. Ecotoxicol Environ Saf 255.
[53] Kolesnik, O.V., Rozhko, T.V., Lapina, M.A., Solovyev, V.S., Sachkova, A.S., Kudryasheva, N.S., 2021. Development of cellular and enzymatic bioluminescent assay systems to study low-dose effects of thorium. Bioengineering 8 (12).
[54] Zhang, J., Liu, S.S., Yu, Z.Y., Zhang, J., 2013. Time-dependent hormetic effects of 1-alkyl-3-methylimidazolium bromide on *Vibrio qinghaiensis* sp.-Q67: luminescence, redox reactants and antioxidases. Chemosphere 91 (4), 462–467.
[55] Esimbekova, E.N., Nemtseva, E.V., Bezrukikh, A.E., Jukova, G.V., Lisitsa, A.E., Lonshakova-Mukina, V.I., et al., 2017. Bioluminescent enzyme inhibition-based assay to predict the potential toxicity of carbon nanomaterials. Toxicol Vitr 45, 128–133.
[56] Kaku, T., Sugiura, K., Entani, T., Osabe, K., Nagai, T., 2021. Enhanced brightness of bacterial luciferase by bioluminescence resonance energy transfer. Sci Rep 11 (1).
[57] Mallevre, F., Fernandes, T.F., Aspray, T.J., 2014. Silver, zinc oxide and titanium dioxide nanoparticle ecotoxicity to bioluminescent Pseudomonas putida in laboratory medium and artificial wastewater. Environ Pollut 195, 218–225.
[58] Wang, D., Bai, L., Li, S., Yan, W., 2022. Similarities and differences in quorum sensing-controlled bioluminescence between *Photobacterium phosphoreum* T3 and *Vibrio qinghaiensis sp.*-Q67. Appl Sci 12 (4).